Letter

ADVANCED PHOTONICS

Perturbation-driven echo-like superfluorescence in perovskite superlattices

Qiangqiang Wang,[a,†] Jiqing Tan,[a,†] Qi Jie,[a] Hongxing Dong,[b,*] Yongsheng Hu,[a] Chun Zhou,[b] Saifeng Zhang,[c] Yichi Zhong,[b] Shuang Liang,[a,d] Long Zhang,[b,e] Wei Xie,[a,f,*] and Hongxing Xu[a,d,*]

[a]East China Normal University, School of Physics and Electronic Science, State Key Laboratory of Precision Spectroscopy, Shanghai, China
[b]Chinese Academy of Sciences, Shanghai Institute of Optics and Fine Mechanics, Key Laboratory of Materials for High-Power Laser, Shanghai, China
[c]Shanghai University, Department of Physics, Shanghai, China
[d]Wuhan University, School of Physics and Technology, Center for Nanoscience and Nanotechnology, Wuhan, China
[e]University of Chinese Academy of Sciences, Hangzhou Institute for Advanced Study, Hangzhou, China
[f]Chongqing Institute of East China Normal University, Chongqing Key Laboratory of Precision Optics, Chongqing, China

Abstract. The collective response of macroscopic quantum states under perturbation is widely used to study quantum correlations and cooperative properties, such as defect-induced quantum vortices in Bose–Einstein condensates and the non-destructive scattering of impurities in superfluids. Superfluorescence (SF), as a collective effect rooted in dipole–dipole cooperation through virtual photon exchange, leads to the macroscopic dipole moment (MDM) in high-density dipole ensembles. However, the perturbation response of the MDM in SF systems remains unknown. Echo-like behavior is observed in a cooperative exciton ensemble under a controllable perturbation, corresponding to an initial collapse followed by a revival of the MDM. Such a dynamic response could refer to a phase transition between the macroscopic coherence regime and the incoherent classical state on a time scale of 10 ps. The echo-like behavior is absent above 100 K due to the instability of MDM in a strongly dephased exciton ensemble. Experimentally, the MDM response to perturbations is shown to be controlled by the amplitude and injection time of the perturbations.

Keywords: superfluorescence; polariton; photoluminescence; exciton.

Received Feb. 22, 2023; revised manuscript received Jul. 24, 2023; accepted for publication Sep. 11, 2023; published online Oct. 6, 2023.

[DOI: 10.1117/1.AP.5.5.055001]

1 Introduction

The phase transition between the macroscopic coherence phase and the incoherent classical regime in a many-body system is an important and fundamental topic in physics.[1–3] Superfluorescence (SF),[4,5] as a cooperative radiation effect originating from initially hot dipoles, is an alternative platform to study such a phase transition involving many-body synchronization in dipole ensembles.[6,7] In the SF process, a macroscopic dipole moment (MDM) is set up from the vacuum quantum fluctuation in a correlated dipole gas,[8] resulting in short and bright light pulses with a radiation duration inversely proportional to the dipole density.[9] MDMs have been realized in several many-body systems,[10,11] such as atomic/molecular gases in optical cells,[12,13] magneto-plasma in two-dimensional quantum wells,[14] nitrogen vacancy centers in diamond crystals,[15,16] excitons in perovskite microstructures,[17,18] and excitons in semiconductor quantum dots (QDs).[19–23] Although MDMs have been demonstrated in a variety of systems, the collapse and reconstruction dynamics for MDMs have not yet been revealed. Even more challenging is the control of the quantum-classical phase transition mentioned above. An alternative method is to actively apply a controllable perturbation to the cooperative ensemble and to study the collective response characteristics of the MDM. Similar methods have been used in other many-body correlated systems, such as defect-induced quantum vortices in polaritonic condensates[24,25] and novel scattering for impurities in superfluids.[26,27] Nevertheless, to date, few studies have reported on the perturbation response of MDM in cooperative dipole ensembles.

*Address all correspondence to Wei Xie, wxie@phy.ecnu.edu.cn; Hongxing Dong, hongxingd@siom.ac.cn; Hongxing Xu, hxxu@whu.edu.cn.

†These authors contributed equally to this work.

Here, by introducing an active perturbation to a correlated exciton ensemble, we reveal the collective response of MDM under a perturbation, i.e., the rapid collapse and revival of MDM. Such a dynamical echo-like evolution has been experimentally demonstrated in spatially localized systems under perturbation, unlike the Burnham–Chiao ringing behavior based on the spontaneous evolution in the absence of perturbation.[22] Here the collapse and revival of MDM corresponds to a phase transition between the many-body quantum regime and the incoherent classical state under perturbation. Such a phase transition is shown to be controllable within a time interval of 10 ps by adjusting the perturbation time and amplitude. Furthermore, when the sample temperature is raised to 100 K, MDM cannot be effectively constructed in the exciton ensemble. Consequently, these collective responses disappear even when the same perturbation is applied.

2 Materials and Methods

All experiments with the $CsPbBr_3$ superlattice sample are required to be performed in a high-vacuum closed-helium-cycle Dewar (MONTANA) at a temperature of 10 K. The excitation source is a femtosecond laser (300 fs, 80 MHz) with a center energy of 3.19 eV. The data in Figs. 1(c)–1(e) are measured using a single-pulse excitation configuration, whereas the other experimental results in the study are obtained using a double-pulse excitation configuration. Detailed experimental configurations are shown in Fig. S2 in the Supplementary Material. The radiation signal is collected through a 50× objective lens [numerical aperture (NA) = 0.55]. The time-integrated PL spectra [Fig. 1(c)] are measured with a spectrometer (ANDOR, Newton, SR500i). The time-resolved PL measurements are obtained using a streak camera with a time resolution of 2 ps (Hamamatsu, C10910). The detailed sample preparation methods and procedures are described in Ref. 23. Some images of the superlattice sample are shown in Fig. S1 in the Supplementary Material. The data in Figs. 2 and 4 are from the same superlattice, and data in Fig. 3 and Fig. S4 in the Supplementary Material are from a different superlattice on the same substrate; both samples are of the same type and are self-assembled QD superlattice microcavities with different lasing thresholds.

3 Results

3.1 Typical Superfluorescence Effect

Our sample is the microsuperlattice assembled by perovskite QDs[23] [Fig. 1(a)]. Recently, the excitons in perovskite nano/

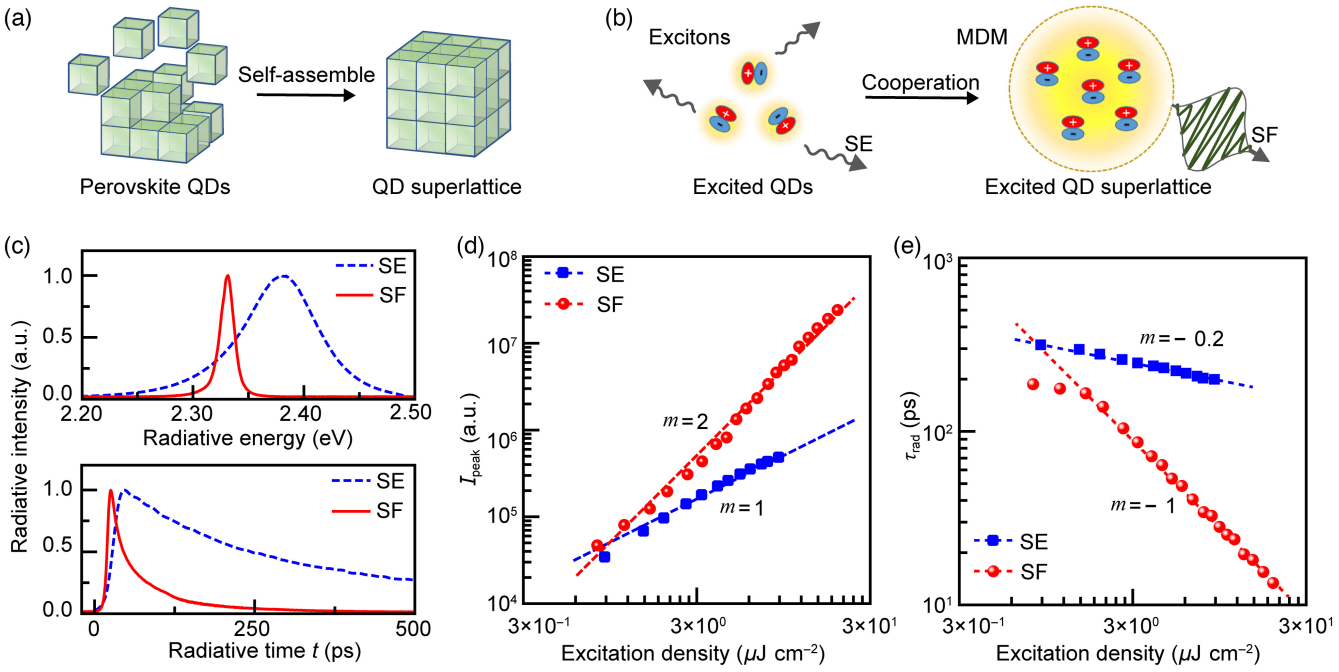

Fig. 1 SF effect in perovskite QD superlattice. (a) Sketch of a superlattice sample assembled by $CsPbBr_3$ QDs. The size of the individual cubic QDs is ~10 nm, and the size of the assembled superlattices is distributed from submicrometers to micrometers. (b) Physical pictures of the excited states and the different radiation effects in corresponding samples. An exciton is shown as a pair of "±," and the MDM is a collective state of a dipole ensemble with an MDM and a synchronous radiation phase. The yellow halo around the "±" pair presents the virtual light field. Dense excitons in a QD superlattice share the virtual light fields and from MDM. Black curved arrows describe the substantial radiation fields, i.e., the SE from individual excitons and the SF from cooperative excitons. (c) Time-integrated and time-resolved spectra. The SE signals from individual QDs and the SF signals from an assembled superlattice are measured under excitation densities of 6.1 and 5.8 $\mu J\,cm^{-2}$ per pulse, respectively. (d), (e) Excitation density ρ versus the time-resolved peak intensity I_{peak} and the radiation decay time τ_{rad}. The dashed lines are guidelines for the trends $y \propto x^m$. I_{peak} and τ_{rad} are obtained by fitting the time-resolved spectra under different excitation densities.

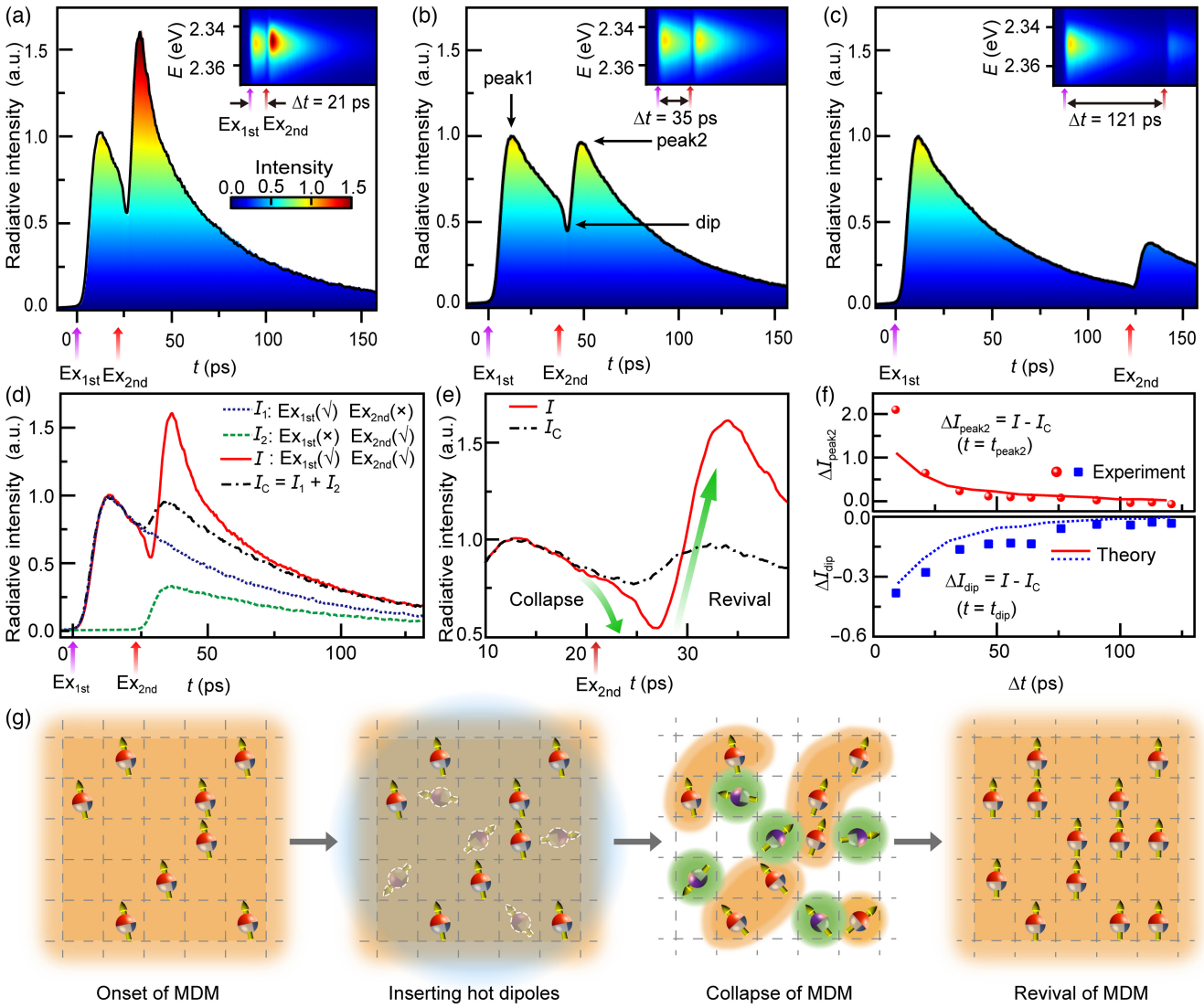

Fig. 2 Echo-like SF behavior under a controllable disturbance. (a)–(c) Time-resolved photoluminescence (PL) spectra at 10 K. The intensities are normalized by the intensity of the first peak. The arrows below the horizontal axis indicate the pulsed excitation times. The pulse densities Ex_{1st} and Ex_{2nd} are fixed at 5.4 and 3 $\mu J\,cm^{-2}$, respectively. The insets show the radiation energy/time-resolved mapping data. The row data at the spectral peak center are extracted and plotted in the corresponding main graph. (d) Comparison of the experimental results (I_1, I_2, I) and the comparison data (I_C). The excitation parameters are the same as those in (a). (e) Zooming in the echo-like part in (d). (f) Disturbance-induced intensity variations (ΔI_{peak2}, ΔI_{dip}) versus the disturbance injection moment (Δt). (g) Physical explanation of the echo-like radiation. The red (purple) spheres represent excitons pumped by Ex_{1st} (Ex_{2nd}). The brown arrows passing across spheres describe the cooperative radiation phase. The blue halo represents the laser field of Ex_{2nd}, which adds new hot excitons to the previous cooperative exciton ensemble. The orange (green) background is the virtual light field shared by the cooperative (hot) excitons. The grid lines represent the QD units in the superlattice sample.

microstructures with long coherence time[28,29] and strong oscillator strength[30,31] have been reported. Here the $CsPbBr_3$ QD superlattice is advantageous for realizing many-body correlation via virtual photon exchange due to the high stacking density of perovskite QDs, the long-range order of the QD arrays, and the low defect density of the superlattice structure (Fig. S1 in the Supplementary Material). Figure 1(b) shows two different effects of two types of QD systems, corresponding to the radiation characteristics of spontaneous emission (SE) from individual excitons and SF from cooperative excitons. Based on the unassembled dispersive QDs, the time-integrated SE spectrum and the time evolution of the spectral peak [Fig. 1(c)] are obtained by a spectroscopy system combined with a streak camera. Meanwhile, the SF signals from an assembled superlattice

are measured at 10 K under nonresonant excitation by a pulsed laser with a duration of 300 fs and a wavelength of 400 nm. The spectral peak in the SF signals is much narrower than that in the SE signals because the QDs in the superlattice sample are more homogeneous than the dispersive QDs without assembly.[23] Furthermore, the radiation decay time τ_{rad} for the SF signals is much shorter than that for the SE signals. In addition, the power dependencies of the transient peak intensities I_{peak} and τ_{rad} are obtained, as shown in Figs. 1(d) and 1(e) in double logarithmic coordinates. Furthermore, Fig. S3 in the Supplementary Material demonstrates that the full width at half-maximum of the SF spectrum exhibits minimal variation with increasing excitation density. Notably, the superlattice sample has a power threshold related to the phase transition from SE to SF ($\rho_{th} \sim 1.6\ \mu J\,cm^{-2}$). Above the threshold, the radiation behavior of the QD superlattice shows a typical dependence on the excitation density ρ, i.e., $\tau_{rad} \propto \rho^{-1}$, $I_{peak} \propto \rho^{2}$. Since the superlattice thickness of 0.5 μm does not support the propagation and reabsorption of SF in the superlattice, no Burnham–Chiao ring is observed in the time-resolved spectrum.

3.2 Superfluorescence Behavior under a Controllable Disturbance

Next, we focus on the response of the cooperative dipole ensemble under disturbance. A double-pulse excitation is applied to combine the many-body cooperation and the phase disturbance in a QD superlattice (for the experimental configuration, see Fig. S2 in the Supplementary Material). The first excitation pulse (Ex_{1st}) is used to trigger the cooperation effect and generate MDM in the exciton ensemble, whereas the second excitation pulse (Ex_{2nd}) is introduced to disturb the MDM. Hot dipoles without a collective phase are introduced into the excited superlattice sample containing the MDM. Accordingly, an echo-like radiation dynamics is observed for the case of a time interval between the two excitation pulses of $\Delta t = 21$ ps [Fig. 2(a)]. In the initial phase, the hot injected dipoles can destroy the collective order of the dipole moments in the previous dipole ensemble. However, in the subsequent period, the cooperation effect is expected to dominate in the correlated dipole system [Fig. 2(g)]. The accessing moment for the disturbance is changed to study the disturbance response in Figs. 2(a)–2(c). Although the disturbance strength (the intensity of the disturbation beam) is fixed, the response changes when Δt increases from 9 to 121 ps, corresponding to a decreasing magnitude for the echo-like signals. The earlier the injection time for Ex_{2nd} is, the larger the magnitude of the MDM that remains in the ensemble to interact with the perturbation, resulting in a stronger feedback response.

Meanwhile, we measured the radiation signals induced by individual excitation pulses [Fig. 2(d)]. Comparative data I_C are plotted by adding the two signals under individual excitations. The apparent differences are between the comparative data I_C and the experimental data I in the magnified picture [Fig. 2(e)]. For quantitative contrast, the intensity variations at the dip moment and at the second peak moment (ΔI_{dip}, ΔI_{peak2}) are shown in Fig. 2(f). After nonresonant excitation by Ex_{2nd}, high-energy carriers are generated and relax incoherently to the low-energy exciton state. This leads to a noticeable collapse of the MDM due to the phase mismatch between the original excitons and the newly inserted excitons [Fig. 2(g)]. However, a reconstructed MDM can emerge due to the cooperative nature of high-density excitons in a low-dephasing situation.

Some comparative effects are discussed below. Note that the echo-like behavior occurs in a short-time window of 10 ps, so many slowly varying effects can be excluded. The duration time for thermal accumulation and diffusion is expected to be longer than 10 ns in the sample composed of individual QDs as the units.[32] Therefore, thermokinetics related to effects cannot match the fast response cycle. In addition, the tunneling of carriers across the nanometer gap between adjacent QDs is also negligible because the tunneling time without bias voltage (>100 ps) is much longer than the echo-like response time in QD superlattices.[33] For the case of $\rho \sim 10\ \mu J\,cm^{-2}$ in the superlattice sample, the average distance between excitons is about 23 nm (details of estimation in Part II in the Supplementary Material), which is less than half the emission wavelength ($\lambda/2 \sim 110$ nm in the medium) and larger than the average size of a single QD (10 nm). The average number of excitons per QD is not more than 0.1. It has been reported that the Auger lifetime of excitons in $CsPbBr_3$ QDs with similar population conditions is on the order of 100 ps,[34] which is 1 order of magnitude larger than the time duration of the echo-like phenomenon. More importantly, the Auger relaxation of the carriers cannot explain the remarkable revival of radiation signals. However, the pure dephasing of the exciton ensemble and the rebuilding process for the MDM by virtual photon exchanges could explain the echo-like behavior. Furthermore, these processes can occur on the time scale of picoseconds. It is shown that the time of cooperation establishment in superlattice samples is shorter than 5 ps in the case of single-pulse excitation.[23] Under double-pulse excitation, the injected excitons disperse into QD lattice points and induce random virtual light fields covering local areas [Fig. 2(g)]. These additional fluctuations break the current equilibrium maintained by the virtual photon exchanges between the original dipoles. Thus the MDM is initially destroyed by the virtual light fluctuations, corresponding to the rapid decrease in radiative intensity. However, in the subsequent period, a new equilibrium of dipole moments would be established by the highly efficient exchange of virtual photons, corresponding to the reconstruction of the MDM and the revival of the radiative signals.

3.3 Temperature Dependence of Echo-Like SF Behavior

The perturbation response of the exciton ensemble is studied at different temperatures (Fig. 3). Interestingly, the disturbance response is closely related to the collective state of the exciton ensemble. The level of cooperation in the exciton ensemble can be controlled by tuning the phonon–exciton scattering rate, i.e., by varying the temperature-dependent phonon density in the QD superlattice. In our sample, the MDM faded away from 10 to 100 K because the dephasing was enhanced by the phonon–exciton scattering [Fig. 3(a) and Fig. S4 in the Supplementary Material]. The dip characteristic in the response signal disappears with increasing temperature [Fig. 3(b)]. The collective correlation of excitons is crucial for observing the collapse and revival of macroscopic coherence in QD superlattices. In the absence of the cooperative effect between dipoles, there is no echo-like response occurring, even under the same perturbation condition.

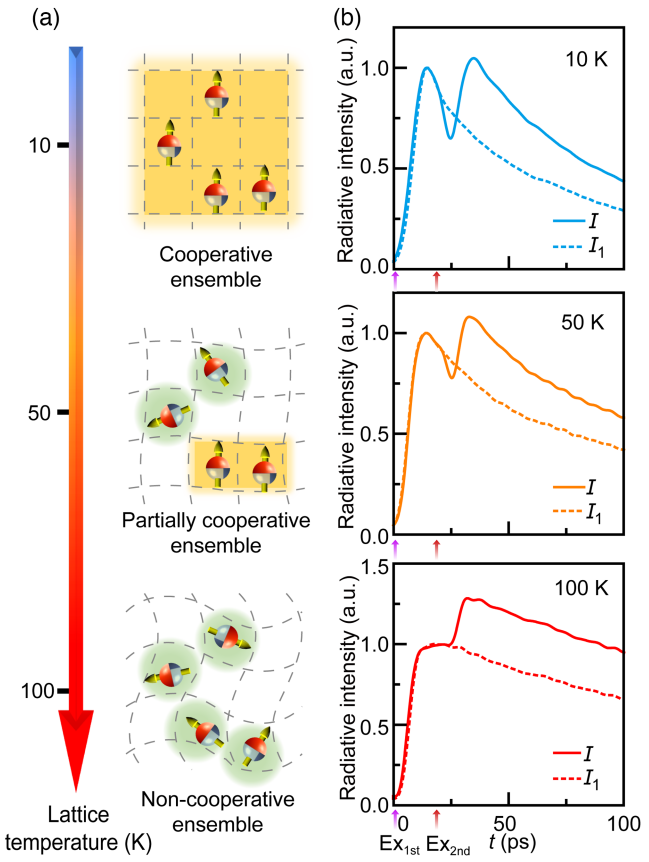

Fig. 3 Echo-like SF behavior versus the temperature of crystal lattice. (a) Temperature-dependent cooperation state of the exciton ensemble, which is determined by the competition of two mechanisms, i.e., the cooperative mechanism via the virtual light field (represented by orange/green background) and the dephasing mechanism via phonon scattering (represented by the twisted lattice). The state of the exciton ensemble changes from "cooperative" at 10 K to "partially cooperative" at 50 K and "noncooperative" at 100 K. (b) Radiation response for an exciton ensemble at different temperatures. The data shown by solid lines are excited by Ex_{1st} and Ex_{2nd} with a fixed pulse density of $\rho_{Ex1} = 5.4\ \mu J\,cm^{-2}$, $\rho_{Ex2} = 2.4\ \mu J\,cm^{-2}$ and an interval time of $\Delta t = 20$ ps. The data shown by dashed lines are excited by Ex_{1st} only.

3.4 Disturbance Intensity Dependence of Echo-Like SF Behavior

In addition, the response signal is examined when the magnitude of the MDM is fixed but the power intensity of the disturbed beam is changed [Fig. 4(a)]. A system with a large MDM magnitude is selected ($\Delta t \sim 10$ ps). The radiation intensities of the dip and the second peak are shown in Fig. 4(b) for quantitative contrast. Interestingly, the most remarkable dip response occurs in the case of a sizable perturbation intensity. This can be explained as follows: the dephasing and rebuilding of the MDM occur together after Ex_{2nd}. When the rates of these two competing effects are approximately equal, the system transitions to the dip state, i.e., the inversion point of the radiation intensity. Thus extreme perturbation cases are unfavorable for remarkable dips. In the case with weak perturbation (e.g., $\rho_{Ex2} = 0.6\ \mu J\,cm^{-2}$), the insert-induced dephasing of MDM is limited. In the case with strong perturbation (e.g., $\rho_{Ex2} = 5.4\ \mu J\,cm^{-2}$), the rebuilding rate increases rapidly to overcome the dephasing process, corresponding to the evanescence of the dip.

4 Discussion

Theoretically, the dynamics of the transition dipole moments σ in the exciton ensemble can be described as follows:[23]

$$\frac{d\sigma}{dt} = -i\omega\sigma + igEN_0\sigma_z - \Gamma_{dp}\sigma + F. \quad (1)$$

In this equation, ω is the transition frequency, and g is the coupling coefficient between the excitons and the optical field E in the superlattice sample. The emission intensity I is proportional to $|E|^2$. N_0 is the number of QDs that can participate in the cooperation effectively. σ_z is the population inversion of the exciton ensemble under the mean-field approximation, i.e., $(\sigma_z + 1)/2 = N/N_0$, where N is the excited number. The term $igN_0E\sigma_z$ contributes a significant gain of σ, and the term $\Gamma_{dp}\sigma$ represents the dephasing/loss of σ with a rate of $\Gamma_{dp} = \Gamma_{phon} + \Gamma_{d-d}N + \Gamma_s\upsilon_{Ex2}$. Γ_{phon} is the phonon–exciton scattering rate, and Γ_{d-d} is the dipole–dipole scattering coefficient of the exciton ensemble. $\Gamma_s\upsilon_{Ex2}$ describes the shock of dephasing rate related to the inserted excitons introduced by Ex_{2nd}, and υ_{Ex2} is the time profile of the number of inserted excitons. Moreover, the virtual photon exchange induces a fluctuation F in the correlated exciton ensemble, whose form is $F^*(t)F(t') = \beta_{vac}N^2\delta(t-t')$, where β_{vac} is the scale parameter for the vacuum quantum fluctuation to trigger cooperation between dipoles. More details are given in Part III in the Supplementary Material.

The term $\Gamma_s\upsilon_{Ex2}$ plays a crucial role in the collapse progress of MDM. As shown in Fig. S6(a) in the Supplementary Material, the simulation results with and without the $\Gamma_s\upsilon_{Ex2}$ term are completely different. Note that the normal scattering terms are reserved, such as the dipole–dipole scattering term $\Gamma_{d-d}N$ in the equation of σ and the Auger scattering term $\kappa_s\upsilon_{Ex2}$ in the equation of exciton number N. The effects of these normal scattering terms are also enhanced after the injection of hot excitons by the second excitation pulse. However, they cannot contribute significantly to I_{dip} [Figs. S6(a) and S6(b) in the Supplementary Material]. Only the $\Gamma_s\upsilon_{Ex2}$ term could induce a transient steep dip signal due to the activation of the collapse of the MDM by the virtual light disturbance. In addition, the term F also plays an important role in the revival region [Figs. S6(c) and S6(d) in the Supplementary Material]. When the term F is removed, the calculated value of I_{peak2} is always significantly smaller than the experimental data, indicating the absence of the revival of MDM. Moreover, this theoretical model could also simulate the experimental data shown in Figs. 2(f) and 4(c).

5 Conclusions

In summary, the collapse and reconstruction of the MDM in perovskite QD-assembled superlattices under an external perturbation is observed, corresponding to 10-ps transitions between the macroscopic coherence phase and the incoherent classical regime. Our work extends the methods of cooperative dipole research to active intervention in many-body correlated ensembles. The ability to control the macroscopic cooperation of dipoles in perovskite microstructures has potential applications in bright pulsed light sources and miniature quantum simulators.

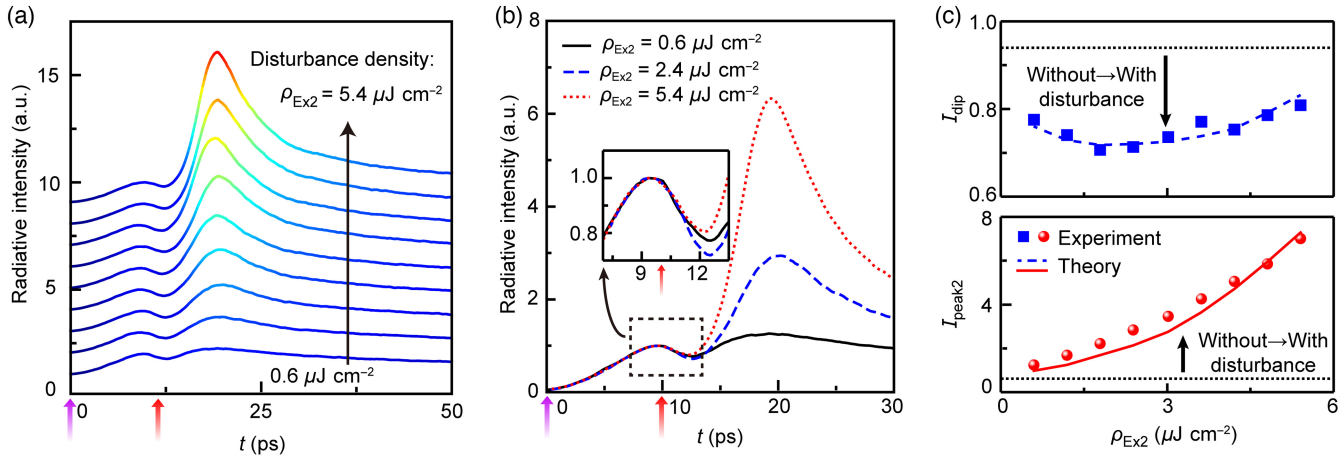

Fig. 4 Echo-like SF behavior versus the disturbance strength. (a) Radiation dynamics for different disturbance amplitudes. Other excitation parameters ($\Delta t = 10$ ps, $T = 10$ K, and $\rho_{Ex1} = 5.4\ \mu J\,cm^{-2}$) are fixed. All curves are normalized to the intensity of the first peak, and each curve is equally spaced along the vertical axis for clarity. (b) Comparison of three disturbance cases. The dip region (dashed box) is further magnified. (c) Echo-like SF versus disturbance amplitude. The radiation intensities without and with the disturbance are shown as black and colored lines, respectively. The largest dip occurs at a moderate disturbance amplitude $\rho_{Ex2} = 1.8\ \mu J\,cm^{-2}$, depending on the competition between scattering dephasing and the rebuilding rate of the MDM.

Data, Materials, and Code Availability

Data underlying the results presented in this paper may be obtained from the authors upon reasonable request.

Acknowledgments

We would like to thank researchers Liaoxin Sun, Zheyu Shi, Keye Zhang, Zheng Sun, Deng Pan, and Prof. Long Zhang for helpful discussions. This work was supported by the Ministry of Science and Technology of China (Grant No. 2021YFA1401100), the National Natural Science Foundation of China (Grant Nos. 12174112, 61925506, 12374297, and 62305078), the Natural Science Foundation of Shanghai (Grant Nos. 23ZR1419800 and 20JC1414605), and Chongqing and Zhejiang Province (Nos. 2023NSCQ-MSX1489 and TD2020002). The authors declare no competing interests. W.X. conceived and designed the optical experiment. Q.W. and J.T. performed the experimental measurements. Q.J. developed the theoretical model, guided by W.X. and H.X. C.Z. and B.Z. fabricated the samples, guided by H.D. All authors discussed the results and wrote the paper.

References

1. A. D. Greentree et al., "Quantum phase transitions of light," *Nat. Phys.* **2**(12), 856–861 (2006).
2. K. Baumann et al., "Dicke quantum phase transition with a superfluid gas in an optical cavity," *Nature* **464**(7293), 1301–1306 (2010).
3. R. Su et al., "Room temperature long-range coherent exciton polariton condensate flow in lead halide perovskites," *Sci. Adv.* **4**(10), eaau0244 (2018).
4. R. H. Dicke, "Coherence in spontaneous radiation processes," *Phys. Rev.* **93**(1), 99–110 (1954).
5. R. Bonifacio and L. A. Lugiato, "Cooperative radiation processes in two-level systems: superfluorescence," *Phys. Rev. A* **11**(5), 1507–1521 (1975).
6. V. V. Temnov and U. Woggon, "Superradiance and subradiance in an inhomogeneously broadened ensemble of two-level systems coupled to a low-Q cavity," *Phys. Rev. Lett.* **95**(24), 243602 (2005).
7. V. N. Pustovit and T. V. Shahbazyan, "Cooperative emission of light by an ensemble of dipoles near a metal nanoparticle: the plasmonic Dicke effect," *Phys. Rev. Lett.* **102**(7), 077401 (2009).
8. J. H. Kim et al., "Fermi-edge superfluorescence from a quantum-degenerate electron-hole gas," *Sci. Rep.* **3**(1), 3283 (2013).
9. G. T. Noe Ii et al., "Giant superfluorescent bursts from a semiconductor magneto-plasma," *Nat. Phys.* **8**(3), 219–224 (2012).
10. D. S. Chemla and J. Shah, "Many-body and correlation effects in semiconductors," *Nature* **411**(6837), 549–557 (2001).
11. L. Zhang et al., "Photonic-crystal exciton-polaritons in monolayer semiconductors," *Nat. Commun.* **9**(1), 713 (2018).
12. A. I. Chumakov et al., "Superradiance of an ensemble of nuclei excited by a free electron laser," *Nat. Phys.* **14**(3), 261–264 (2018).
13. H. Zhao et al., "Strong optical response and light emission from a monolayer molecular crystal," *Nat. Commun.* **10**(1), 5589 (2019).
14. Y. D. Jho et al., "Cooperative recombination of a quantized high-density electron-hole plasma in semiconductor quantum wells," *Phys. Rev. Lett.* **96**(23), 237401 (2006).
15. C. Bradac et al., "Room-temperature spontaneous superradiance from single diamond nanocrystals," *Nat. Commun.* **8**(1), 1205 (2017).
16. A. Angerer et al., "Superradiant emission from colour centres in diamond," *Nat. Phys.* **14**(12), 1168–1172 (2018).
17. I. Cherniukh et al., "Perovskite-type superlattices from lead halide perovskite nanocubes," *Nature* **593**(7860), 535–542 (2021).
18. M. Biliroglu et al., "Room-temperature superfluorescence in hybrid perovskites and its origins," *Nat. Photonics* **16**(4), 324–329 (2022).
19. M. Scheibner et al., "Superradiance of quantum dots," *Nat. Phys.* **3**(2), 106–110 (2007).
20. Z. J. Ning et al., "Quantum-dot-in-perovskite solids," *Nature* **523**(7560), 324–328 (2015).
21. F. Jahnke et al., "Giant photon bunching, superradiant pulse emission and excitation trapping in quantum-dot nanolasers," *Nat. Commun.* **7**(1), 11540 (2016).

22. G. Raino et al., "Superfluorescence from lead halide perovskite quantum dot superlattices," *Nature* **563**, 671–675 (2018).
23. C. Zhou et al., "Cooperative excitonic quantum ensemble in perovskite-assembly superlattice microcavities," *Nat. Commun.* **11**(1), 329 (2020).
24. K. G. Lagoudakis et al., "Observation of half-quantum vortices in an exciton-polariton condensate," *Science* **326**(5955), 974–976 (2009).
25. T. Torres et al., "Rotational superradiant scattering in a vortex flow," *Nat. Phys.* **13**(9), 833–836 (2017).
26. L. Jiang et al., "Single impurity in ultracold Fermi superfluids," *Phys. Rev. A* **83**(6), 061604 (2011).
27. D. Cho et al., "A strongly inhomogeneous superfluid in an iron-based superconductor," *Nature* **571**(7766), 541–545 (2019).
28. M. A. Becker et al., "Long exciton dephasing time and coherent phonon coupling in $CsPbBr_2Cl$ perovskite nanocrystals," *Nano Lett.* **18**(12), 7546–7551 (2018).
29. H. Utzat et al., "Coherent single-photon emission from colloidal lead halide perovskite quantum dots," *Science* **363**(6431), 1068–1072 (2019).
30. R. Su et al., "Observation of exciton polariton condensation in a perovskite lattice at room temperature," *Nat. Phys.* **16**(3), 301–306 (2020).
31. Q. A. Akkerman et al., "Controlling the nucleation and growth kinetics of lead halide perovskite quantum dots," *Science* **377**(6613), 1406–1412 (2022).
32. Q. Li et al., "Tracking single quantum dot and its spectrum in free solution with controllable thermal diffusion suppression," *Anal. Biochem.* **377**(2), 176–181 (2008).
33. A. Tackeuchi et al., "Dynamics of carrier tunneling between vertically aligned double quantum dots," *Phys. Rev. B* **62**(3), 1568–1571 (2000).
34. Y. Wang et al., "All-inorganic colloidal perovskite quantum dots: a new class of lasing materials with favorable characteristics," *Adv. Mater.* **27**(44), 7101–7108 (2015).
35. G. Findik et al., "High-temperature superfluorescence in methyl ammonium lead iodide," *Nat. Photonics* **15**(9), 676–680 (2021).
36. J. Liang, J. Liu, and Z. Jin, "All-inorganic halide perovskites for optoelectronics: progress and prospects," *Solar RRL* **5**(10), 1700086 (2017).

Qiangqiang Wang received his PhD in optics from East China Normal University in 2023. He is a researcher in the field of semiconductor optics, with a primary focus on investigating the superfluorescent properties of perovskite materials and developing innovative methods for their active control. His research endeavors aim to provide a deeper understanding of the fluorescence characteristics of perovskite materials, contributing to advancements in the field of optics.

Jiqing Tan is a PhD student in optics at East China Normal University. His research mainly focuses on the exciton dynamics in perovskite materials, optical field manipulation, and numerical simulation and experimentation of laser processing. He has been dedicated to elucidating and advancing the theoretical and experimental methods for the interaction between lasers and matter.

Biographies of the other authors are not available.